Orians KJ, Boyle EA and Bruland KW (1990) Dissolved titanium in the open ocean. *Nature* 348: 322–325.
Roy-Barman M, Chen JH and Wasserburg GJ (1996) 230Th–232Th systematics in the central Pacific Ocean: the sources and the fates of thorium. *Earth and Planetary Science Letters* 139: 351–363.
Shiller AM (1998) Dissolved gallium in the Atlantic Ocean. *Marine Chemistry* 61: 87–99.
Sohrin Y, Fujishima Y, Ueda K *et al.* (1998) Dissolved niobium and tantalum in the North Pacific. *Geophysical Research Letters* 25: 999–1002.
Spencer DW, Robertson DE, Turekian KK and Folsom TR (1970) Trace element calibrations and profiles at the GEOSECS test station in the Northeast Pacific Ocean. *Journal of Geophysical Research* 75: 7688.
Taylor SR (1964) Abundance of chemical elements in the continental crust: a new table. *Geochimica et Cosmochimica Acta* 28: 1273–1285.
Whitfield M and Turner DR (1987) The role of particles in regulating the composition of seawater. In: Stumm W (ed.) *Aquatic Surface Chemistry*, Ch. 17, pp. 457–493. New York: Wiley-Interscience.

REGIONAL AND SHELF SEA MODELS

J. J. Walsh, University of South Florida, St Petersburg, Florida, USA

doi:10.1006/rwos.2001.0399

Introduction

Simple biological models of nutrient (N), phytoplankton (P), and zooplankton (Z) state variables were formulated more than 50 years ago (Riley *et al.*, 1949), with minimal physics, to explore different facets of marine plankton dynamics. These N–P–Z models, usually in units of nitrogen or carbon are still used in coupled biophysical models of ocean basins, where computer constraints preclude the use of more complex ecological formulations of global biogeochemical budgets. At the regional scale (**Table 1**) of individual continental shelves (Steele, 1974; Walsh, 1988), however, pressing questions no longer focus on the amount of biomass of the total phytoplankton community, but are instead concerned with the functional types of algal species that may continue to support fisheries, generate anoxia, fix nitrogen, or form toxic red tides.

Regional models that presently address the outcome of such plankton competition must of course specify the rules of engagement among distinct functional groups of P, Z, and larval fish (F) living and dying within time-dependent physical (e.g., light, temperature, and current) and chemical (e.g., N) habitats. Successful ecological models are data-driven, distilling qualitative hypotheses and aliased field observations into simple analogs of the real world in a continuing cycle of model testing and revision. They are usually formulated as part of multidisciplinary field studies, in which the temporal and spatial distributions of the model's state variables, from water motion to plankton abundances, are measured to provide validation data. Here, examples of some state-of-the-art, complex regional biophysical models are drawn from specific field programs designed to validate them. Depending upon the questions asked of regional models, processes at smaller and larger time/space scales (**Table 1**) are variously ignored, parametrized, or specified as boundary conditions.

Statistical models elicit noncausal relationships among presumed independent variables with poorly known probability density functions. Deterministic simulation models in contrast assign cause and effect among the state variables and forcing functions described by a set of usually nonlinear ordinary or partial differential equations, whose solutions are obtained numerically. Within a fluid subjected to such external forcing, the vagaries of population changes of the embedded plankton, along measured spatial gradients, must be described in relation to both water motion and biotic processes.

For example, in a Lagrangian sense – following the motion of a parcel of fluid – the time dependence of larval fish (F) can be written simply as an ordinary differential equation (eqn [1]), where the total derivative is given by eqn [2].

$$\frac{\mathrm{d}F}{\mathrm{d}t} = (b - d)F \qquad [1]$$

$$\frac{\mathrm{d}}{\mathrm{d}t} = \frac{\partial}{\partial t} + u\frac{\partial}{\partial x} + v\frac{\partial}{\partial y} + w\frac{\partial}{\partial z} \qquad [2]$$

Mixing is ignored and biotic factors are just the linear birth, b, and death, d, rates of the fish. Because drogues have difficulty following plankton patches, and current meters measure flows at a few fixed locations, it is usually more convenient to

Table 1 Domains of ecological and physical processes within a hierarchy of coupled models

Model	*Time domain*	*Space domain*	*Ecological focus*	*Physical focus*
Small scale	Seconds	mm–cm	Cellular metabolism	Dissipation, nutrient supply
Turbulent	Minutes	dm–m	Photoadaptation, cell quotas	Waves, Langmuir cells
Local	Hours	m	Plankton migration, cell division	Tides, inertial oscillations
Regional	Days–weeks	km	Food web interactions, populations, resuspension events, nutrient depletion, grazing controls	Trapped waves, storms, upwelling, frontal currents
Basin	Months	degree (latitude)	Seasonal succession, mammal migration, carbon sequestration	Gyre flows, changes of mixed layer depths
Global	Years	Planetary	Stock fluctuations	Thermohaline circulation
Geological	Centuries	–	Evolution, sedimentation	Climate change

model circulation and the coupled biological fields in an Eulerian sense – over a grid mesh of spatial cells.

The underlying physical models (Csanady, 1982; Heaps, 1987; Mooers, 1998) have a rich history, since the development of calculus by Isaac Newton and Gottfried Leibnitz *c.* 1675, allowing expression of the rates of change, or derivatives, of properties over both time and space. After 1800, for example, Newton's second law of motion became transformed into the time (t)-dependent Navier–Stokes equations for the horizontal (u, v) and vertical (w) motions of a fluid, as a function of density (ρ), pressure (p), gravitational ($g\rho/\rho_0$, where ρ_0 is a reference density), and Coriolis ($fv, -fu, 0$) forces, in a Cartesian coordinate system (x, y, z) as eqns [3]–[5].

$$\frac{\partial u}{\partial t} + u\frac{\partial u}{\partial x} + v\frac{\partial u}{\partial y} + w\frac{\partial u}{\partial z} = \frac{\partial}{\partial x}\left(K_x\frac{\partial u}{\partial x}\right) + \frac{\partial}{\partial y}\left(K_y\frac{\partial u}{\partial y}\right) + \frac{\partial}{\partial z}\left(K_z\frac{\partial u}{\partial z}\right) - \frac{1}{\rho}\frac{\partial \varphi_e}{\partial x} - \frac{1}{\rho}\frac{\partial \varphi_\rho}{\partial x} + fv \quad [3]$$

$$\frac{\partial v}{\partial t} + u\frac{\partial v}{\partial x} + v\frac{\partial v}{\partial y} + w\frac{\partial v}{\partial z} = \frac{\partial}{\partial x}\left(K_x\frac{\partial v}{\partial x}\right) + \frac{\partial}{\partial y}\left(K_y\frac{\partial v}{\partial y}\right) + \frac{\partial}{\partial z}\left(K_z\frac{\partial v}{\partial z}\right) - \frac{1}{\rho}\frac{\partial \varphi_e}{\partial y} - \frac{1}{\rho}\frac{\partial \varphi_\rho}{\partial y} - fu \quad [4]$$

$$\frac{\partial w}{\partial t} + u\frac{\partial w}{\partial x} + v\frac{\partial w}{\partial y} + w\frac{\partial w}{\partial z} = \frac{\partial}{\partial x}\left(K_x\frac{\partial w}{\partial x}\right) + \frac{\partial}{\partial y}\left(K_y\frac{\partial w}{\partial y}\right) + \frac{\partial}{\partial z}\left(K_z\frac{\partial w}{\partial z}\right) - \frac{1}{\rho}\frac{\partial \varphi_\rho}{\partial z} - \frac{g\rho}{\rho_0} \quad [5]$$

subject to appropriate boundary conditions at the surface (s), bottom (b), and sides of the ocean.

For example, the surface wind and bottom friction stresses, $\tau_{s,b}$, are part of the boundary conditions for the third term of internal vertical Reynolds stresses, involving K_z on the right side of eqns [3]–[5]. No water moves across the land interfaces of the first two terms, representing horizontal turbulent mixing at smaller length scales than those of the flow components (u, v, w) over longer timescales. The last three terms on the left side of eqns [3]–[5] are thus the nonlinear advection of momentum in the horizontal and vertical directions, while the first one is the local time change.

In terms of other forces exerting acceleration of the fluid on the right side of eqns [3]–[5], their last terms represent the impact of Coriolis (f) and gravitational (g) effects. The fourth and fifth terms of eqns [3] and [4] are the respective pressure forces exerted by the piled-up mass of sea water (φ_e) (i.e., the barotropic force from slope of the sea surface, e, and the baroclinic one (φ_ρ) from the density field, ρ, which in turn is a function of temperature, (T), salinity (S), and pressure. At the surface of the sea, it is given simply by eqn [6], where ρ_0 is a reference density of pure water and γ is a polynomial function of S and T.

$$\rho = \rho_0 + \gamma(S, T) \quad [6]$$

As in the case of momentum, the time-dependent spatial distributions of these conservative parameters of temperature and salinity are described by equations [7] and [8].

$$\frac{\partial T}{\partial t} + u\frac{\partial T}{\partial x} + v\frac{\partial T}{\partial y} + w\frac{\partial T}{\partial z} = \frac{\partial}{\partial x}\left(K_x\frac{\partial T}{\partial x}\right) + \frac{\partial}{\partial y}\left(K_y\frac{\partial T}{\partial y}\right) + \frac{\partial}{\partial z}\left(K_z\frac{\partial T}{\partial z}\right) \quad [7]$$

$$\frac{\partial S}{\partial t} + u\frac{\partial S}{\partial x} + v\frac{\partial S}{\partial y} + w\frac{\partial S}{\partial z} = \frac{\partial}{\partial x}\left(K_x\frac{\partial S}{\partial x}\right)$$

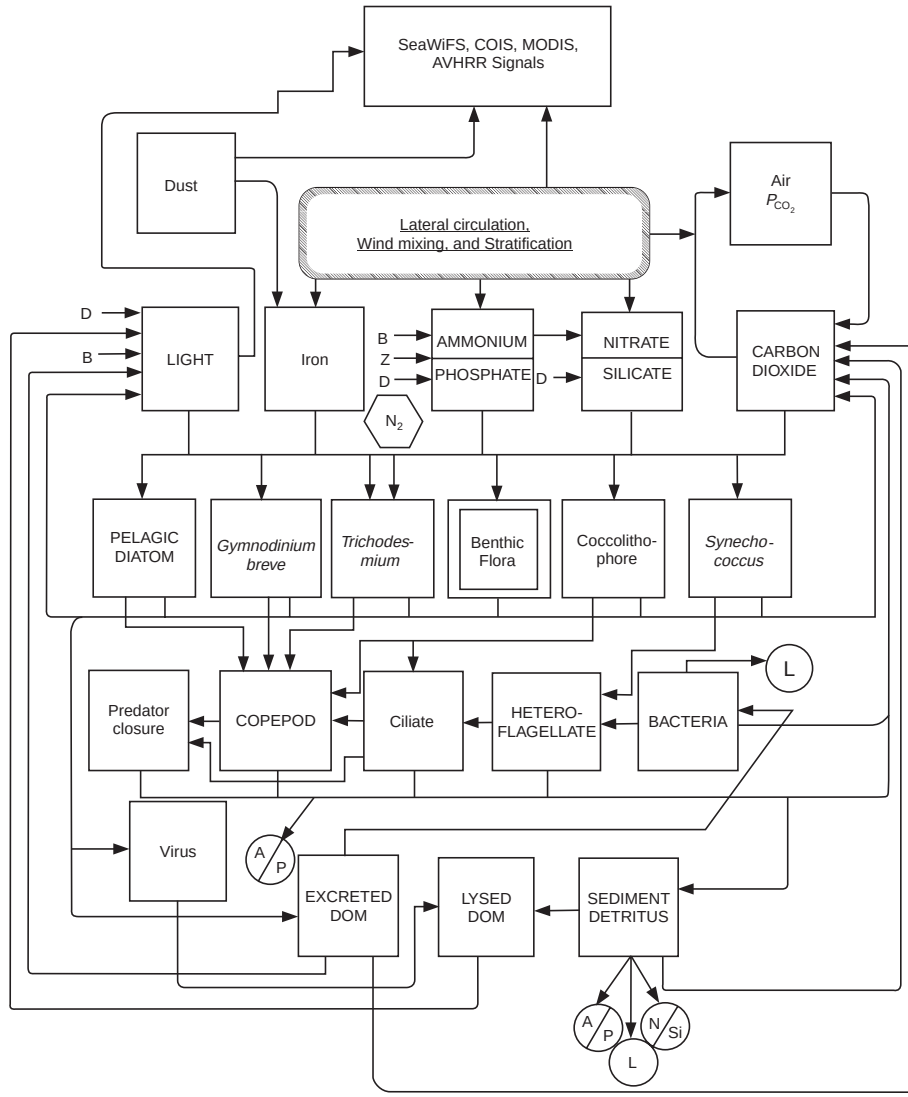

Figure 1 State variables of an ecologically complex numerical food web, coupled to a physical model of water circulation, for analysis of phytoplankton competition leading both to harmful algal blooms of *Gymnodinium breve* and to larval fish predators on the West Florida shelf.

$$+\frac{\partial}{\partial y}\left(K_y\frac{\partial S}{\partial y}\right)+\frac{\partial}{\partial z}\left(K_z\frac{\partial S}{\partial z}\right) \qquad [8]$$

The different forcings of net incident radiation, latent/sensible heat losses, precipitation, and evaporation at the sea surface are boundary conditions for the last terms on the right side of eqns [7] and [8]. Depending upon the time and space scales of interest (**Table 1**), the coefficients K_x, K_y, and K_z may represent either molecular diffusion, turbulence, viscosity, tidal stirring, or eddy mixing processes, while u, v, and w are obtained from solutions of [3]–[5] and [9] (below).

Finally, to complete description of the physical habitat, conservation of momentum is invoked as the continuity equation [9] by assuming that sea water is an incompressible fluid.

$$\frac{\partial u}{\partial x}+\frac{\partial v}{\partial y}+\frac{\partial w}{\partial z}=0 \qquad [9]$$

Thomas Malthus's consideration of exponential population growth in *c.* 1800 was placed in a marine context of eqn [1] during the 1920s, after recognition of the sources of variation of stock recruitment. Since then, quantitative description of the fluctuations of larval fish abundance have expanded to simple marine food webs (**Figure 1**) that support these vertebrates. State equation [10] for fish now has mixing and a nonlinear term for

zooplankton prey, which are linked to N, P, bacteria (B), dissolved organic matter (D), and benthic microbiota (M) in eqns [11]–[16], where the advective and diffusive terms of eqns [10]–[16] are analogous to those of eqns [3]–[5].

$$\frac{\partial F}{\partial t} + u\frac{\partial F}{\partial x} + v\frac{\partial F}{\partial y} + w\frac{\partial F}{\partial z} = \frac{\partial}{\partial x}\left(K_x\frac{\partial F}{\partial x}\right) + \frac{\partial}{\partial y}\left(K_y\frac{\partial F}{\partial y}\right) + \frac{\partial}{\partial z}\left(K_z\frac{\partial F}{\partial z}\right) + (bZ - d)F \quad [10]$$

$$\frac{\partial Z}{\partial t} + u\frac{\partial Z}{\partial x} + v\frac{\partial Z}{\partial y} + w\frac{\partial Z}{\partial z} = \frac{\partial}{\partial x}\left(K_x\frac{\partial Z}{\partial x}\right) + \frac{\partial}{\partial y}\left(K_y\frac{\partial Z}{\partial y}\right) + \frac{\partial}{\partial z}\left(K_z\frac{\partial Z}{\partial z}\right) + (\alpha aP + cB - e - \varepsilon_1 - \delta_1 - bF)Z \quad [11]$$

$$\frac{\partial P}{\partial t} + u\frac{\partial P}{\partial x} + v\frac{\partial P}{\partial y} + w\frac{\partial P}{\partial z} = \frac{\partial}{\partial x}\left(K_x\frac{\partial P}{\partial x}\right) + \frac{\partial}{\partial y}\left(K_y\frac{\partial P}{\partial y}\right) + \frac{\partial}{\partial z}\left(K_z\frac{\partial P}{\partial z}\right) + (gN - \varepsilon_2 - \delta_2 - aZ)P + w_p\frac{\partial P}{\partial z} \quad [12]$$

$$\frac{\partial B}{\partial t} + u\frac{\partial B}{\partial x} + v\frac{\partial B}{\partial y} + w\frac{\partial B}{\partial z} = \frac{\partial}{\partial x}\left(K_x\frac{\partial B}{\partial x}\right) + \frac{\partial}{\partial y}\left(K_y\frac{\partial B}{\partial y}\right) + \frac{\partial}{\partial z}\left(K_z\frac{\partial B}{\partial z}\right) + (hD - \delta_3 - cZ)B \quad [13]$$

$$\frac{\partial N}{\partial t} + u\frac{\partial N}{\partial x} + v\frac{\partial N}{\partial y} + w\frac{\partial N}{\partial z} = \frac{\partial}{\partial x}\left(K_x\frac{\partial N}{\partial x}\right) + \frac{\partial}{\partial y}\left(K_y\frac{\partial N}{\partial y}\right) + \frac{\partial}{\partial z}\left(K_z\frac{\partial N}{\partial z}\right) + \frac{\varepsilon_1}{\delta_1}Z + \delta_2 P + \delta_3 B + \frac{\partial}{\partial z}\left(K_z\frac{\partial M}{\partial z}\right) - gNP \quad [14]$$

$$\frac{\partial D}{\partial t} + u\frac{\partial D}{\partial x} + v\frac{\partial D}{\partial y} + w\frac{\partial D}{\partial z} = \frac{\partial}{\partial x}\left(K_x\frac{\partial D}{\partial x}\right) + \frac{\partial}{\partial y}\left(K_y\frac{\partial D}{\partial y}\right) + \frac{\partial}{\partial z}\left(K_z\frac{\partial D}{\partial z}\right) + (1 - \alpha aP) + \varepsilon_2 P + \frac{\partial}{\partial z}\left(K_z\frac{\partial M}{\partial z}\right) - hDB \quad [15]$$

$$\frac{\partial M}{\partial t} + w_z\frac{\partial eZ}{\partial z} + w_p\frac{\partial P}{\partial z} - \frac{\partial}{\partial z}\left(K_z\frac{\partial M}{\partial z}\right) \quad [16]$$

Thus far, F has represented various larval fish species subjected to the vagaries of the currents, of their supply of zooplankton prey (bZF), and of losses (dF) to predators. The simulated Z are a more diverse zooplankton group of protozoans, salps, copepods, and euphausiids, however, while P are numerous functional groups of light-regulated phytoplankton, e.g., the silicate-requiring diatoms, nitrogen-fixing diazotrophs, calcium-using coccolithophores, sulfur-releasing prymnesiophytes, and heavily-grazed chlorophytes, cyanophytes, and cryptophytes of the microbial food web.

Accordingly, the types of inorganic nutrients that have been modeled with eqn [14] are total carbon dioxide, nitrate, ammonium, dinitrogen gas, iron, silicate, calcium, and phosphate, while the dissolved organic matter (DOM) pools have been those of carbon, nitrogen, phosphorus, and sulfur, to provide sufficient algal niches. The particulate pools of the phytoplankton are usually chlorophyll (chl) biomass, or their elemental equivalents. Finally, B are ammonifying and nitrifying bacteria, and M represents both microflora and microfauna, as well as particulate and dissolved debris of the sediments.

The other biological terms of eqns [11]–[16] involve non-linear rate processes, in units of reciprocal time and associated with the various coefficients, such as in the temperature-dependent grazing of phytoplankton by zooplankton (aPZ). Their sloppy feeding is represented by α such that both the herbivores and the phytoplankton excretion ($\varepsilon_2 P$) are sources of the DOM consumed by the bacteria (hDB), who in turn are eaten by other smaller zooplankton (cBZ). Some of the ingested food is released as egested fecal pellets (eZ) to sink (w_z), together with settling phytodetritus ($w_p\,\partial P/\partial z$) to the seafloor. Ammonium and phosphorus are excreted ($\varepsilon_1 Z$) by the respiring ($\delta_1 Z$) grazers as one source of recycled nutrients (including carbon dioxide), as well as those derived from respiring phytoplankton ($\delta_2 P$) and bacteria ($\delta_3 B$) and sediment releases $\partial/\partial z(K_z\partial M/\partial z)$. Finally, the temperature-dependent, light-regulated uptake of nutrients and subsequent growth (gNP) of the phytoplankton is usually a Liebig's law of the minimum formulation, involving saturation kinetics of the available resources, as function of cell quota and a ratio of the required elements.

The respective exchanges of biogenic gases, dissolved solutes, and bioturbated particulate matter across either the air–sea or water–sediment interfaces have been treated as part of the boundary conditions for the vertical diffusive term of these ecological state variables, similarly to the physical formulations of wind stress, bottom friction, and

buoyancy fluxes. Further, since few elements escape the planet, a conservation of mass within marine food webs is also invoked as eqn [17], like that of eqn [9] for momentum.

$$\frac{dF}{dt} + \frac{dZ}{dt} + \frac{dP}{dt} + \frac{dB}{dt} + \frac{dN}{dt} + \frac{dD}{dt} + \frac{dM}{dt} = 0 \quad [17]$$

Model Hierarchies

Despite extensive *in situ* and satellite validation data for today's nonlinear biophysical models, based on some or all of state equations [3]–[17], the models still have numerical problems, since any set of coupled partial differential equations is solved iteratively at each individual grid point of a spatial three-dimensional mesh (**Figure 2**), using time-dependent forcing functions. The smaller the spatial grid mesh and the larger the number of state variables (**Figure 1**), the more computer memory is required, such that any one model must be formulated to provide only a few answers to a hierarchy of possible questions (**Table 1**) – *ergo*, the reason for construction of regional models.

For example, 50 years after the pioneer studies of Riley and co-workers, the present general circulation models (GCMs) still have minimal ecological realism with just nitrate and the total phytoplankton community to allow spatial meshes of $\sim 1/3^{\circ}$ resolution of important physical processes of eddy mixing within basin simulations over ~ 37 depth levels. Ideally, future GCMs may include more biogeochemical state variables to explicitly link

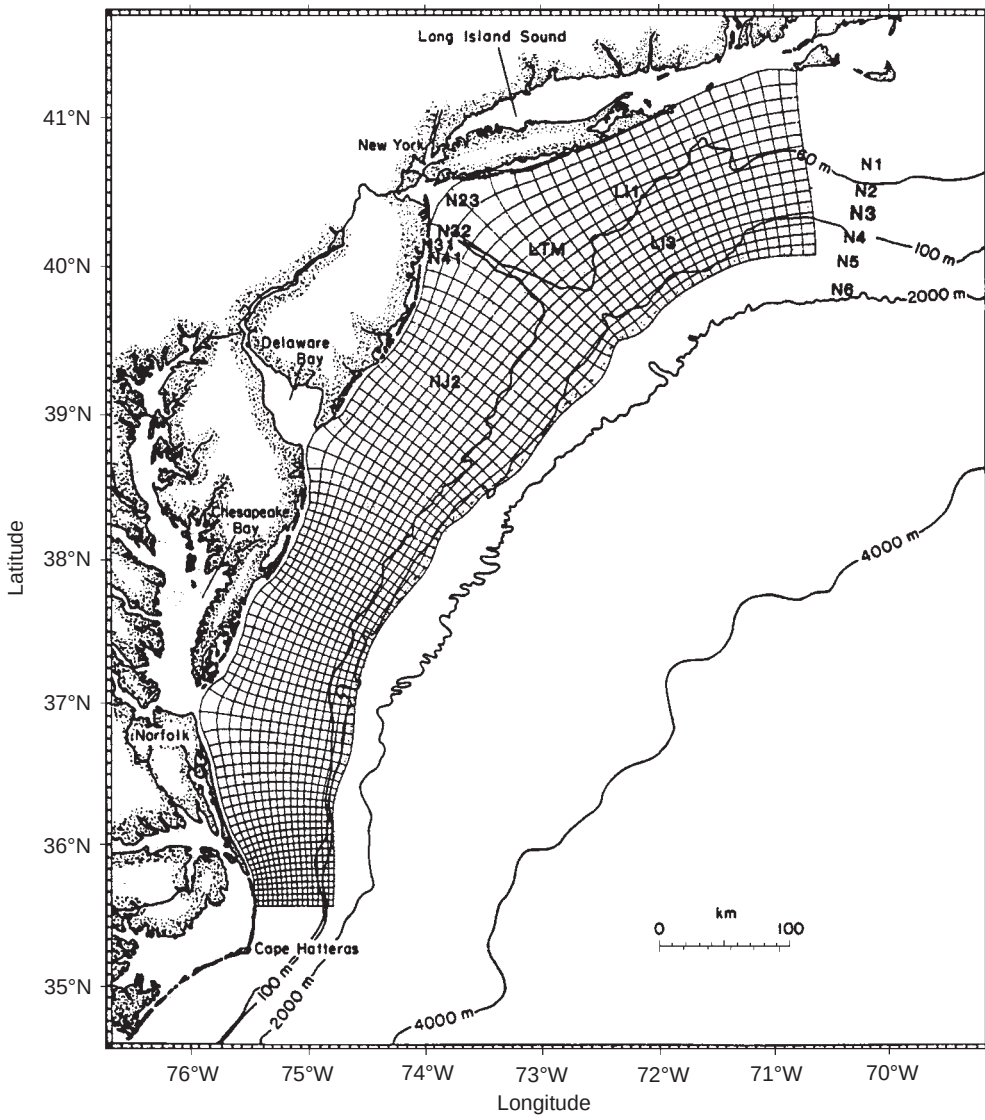

Figure 2 A curvilinear grid, showing every other grid line, of the first coupled physical-biochemical model of the Mid-Atlantic Bight, in relation to upstream (N1–N6) and interior (LI 1, LI 3, LTM, N23, N31–32. N41, and NJ2) current meter moorings.

carbon uptake during net photosynthesis with associated element cycles, e.g., nitrogen fixation, dimethyl sulfide evasion, organic phosphorus lability, calcification, and silica depletion in global budgets of climate change. But present questions of predicting the onset of harmful algal blooms, of the consequences of overfishing regional stocks, and of the fate of eutrophied coastal ecosystems require circulation models at smaller spatial resolution and biological models of greater ecological realism than those of GCMs (**Table 1** and **Figure 1**).

Regional models both incorporate local processes at the high end of their time/space scales of hours and decimeters and extend into the low end of basin models at resolution of months and degrees (**Table 1**). At a residual flow of $5\,\mathrm{cm\,s^{-1}}$, or $\sim 5\,\mathrm{km\,d^{-1}}$, it would take a plankton population about 8 weeks to drift $\sim 300\,\mathrm{km}$ across a region of $\sim 1\times10^{5}\,\mathrm{km^2}$ area, about the size of the Mid-Atlantic Bight, the southern Caribbean Sea, or the West Florida shelf. With a large set of ecological variables (**Figure 1**), however, present computer resources barely allow computation of the terms of eqns [3]–[17] over the $\sim 4\,\mathrm{km}$ resolution of a regional circulation model (**Figure 2**), with ~ 10 depth layers. Thus the complexities of turbulent flows and cellular metabolism must be glossed over, while the results of the regional model cannot be extrapolated over $\sim 3\times10^{7}\,\mathrm{km^2}$ of an adjacent basin without the loss of additional realism.

At the global ocean level of $\sim 3.7\times10^{8}\,\mathrm{km^2}$, lateral boundary conditions of a GCM are not a problem, because land boundaries are specified and flows are computed throughout all sectors of the simulated ocean; surface boundary conditions are another story, requiring input from some atmospheric model! In a regional model of the shelf seas, however, three open boundary conditions must be specified, which determine the solution over the grid mesh of the region of interest. Various options are (1) to use data at some of the boundaries, (2) to move them far way with a telescoping grid mesh, or (3) to make some assumptions about the water flows and fluxes of elements across the boundaries from other models. Examples of results from coupled biophysical models of three shelf regions are shown, using each of these options.

Regional Case Studies

Mid-Atlantic Bight

The first set of coupled biophysical models of the continental shelf and slope of the Mid-Atlantic Bight (MAB) between Martha's Vineyard and Cape Hatteras used the same circulation model, which was wind-forced, with current meter data specifying flows at the upstream boundary (**Figure 2**). The horizontal grid mesh was an average of $\sim 4\,\mathrm{km}$, with analytical solutions yielding continuous vertical profiles of the barotropic flow fields, from the shallow water formulation of the depth-averaged Navier–Stokes equations. During spring conditions of minimal density structure, the barotropic flow is $\sim 90\%$ of the total transport, and the simulated flows of the model exhibited a vector error of $1–2\,\mathrm{cm\ s^{-1}}$ speed and 10–30° direction, compared to the observed currents at interior moorings (**Figure 2**). During a strong upwelling event (**Table 1**), when nutrient-rich subsurface water moves up into the sunlit euphotic zone, the model's vertical velocity, w from eqn [9], was $9–14\,\mathrm{m\,d^{-1}}$ for effecting both supply of unutilized nutrients in eqn [14] and resuspension of settled-out phytoplankton (**Figure 3A**) in eqn [12].

In the first version of a coupled biological model of the MAB, only three vertical levels of ecological interactions were computed within the spatial mesh of the circulation model, with a minimal realism of just nitrate and the whole phytoplankton community as state variables, forced in turn by incident light and time-dependent grazing stress. Within parts of the MAB, this study of 'new' nitrate-based production yielded similar chlorophyll stocks of phytoplankton on 10 April 1979 (**Figure 3B**), after such an upwelling event, to those seen concurrently by a color-sensing satellite (**Figure 3A**) (the Coastal Zone Color Scanner (CZCS)) and an *in situ* moored fluorometer, moored south of Long Island, i.e., between New Jersey and Martha's Vineyard, as well as off Cape Hatteras. At mid-shelf in the wider, central region of the MAB, however, the simulated surface stocks of the first model overestimated those seen by the CZCS.

In another version of the coupled model of both shelf and slope domains, temperature-dependent growth of two groups of phytoplankton (net plankton diatoms and nanoplankton flagellates) utilized both nitrate and ammonium over 10 depth intervals, allowing calculation of the total ('new' + 'recycled') primary production. With the more heavily grazed nanoplankton dominating on the outer shelf and slope, the simulated stocks on 10 April 1979 (**Figure 3C**) now more closely approximated those estimated from the CZCS (**Figure 3A**). The model's total net photosynthesis over March–April was then within 28–97% of the ^{14}C measurements of productivity, depending upon the area and month. A mean of $0.5\,\mathrm{g\,C\,m^{-2}\,d^{-1}}$ suggested that only $\sim 13\%$ of the

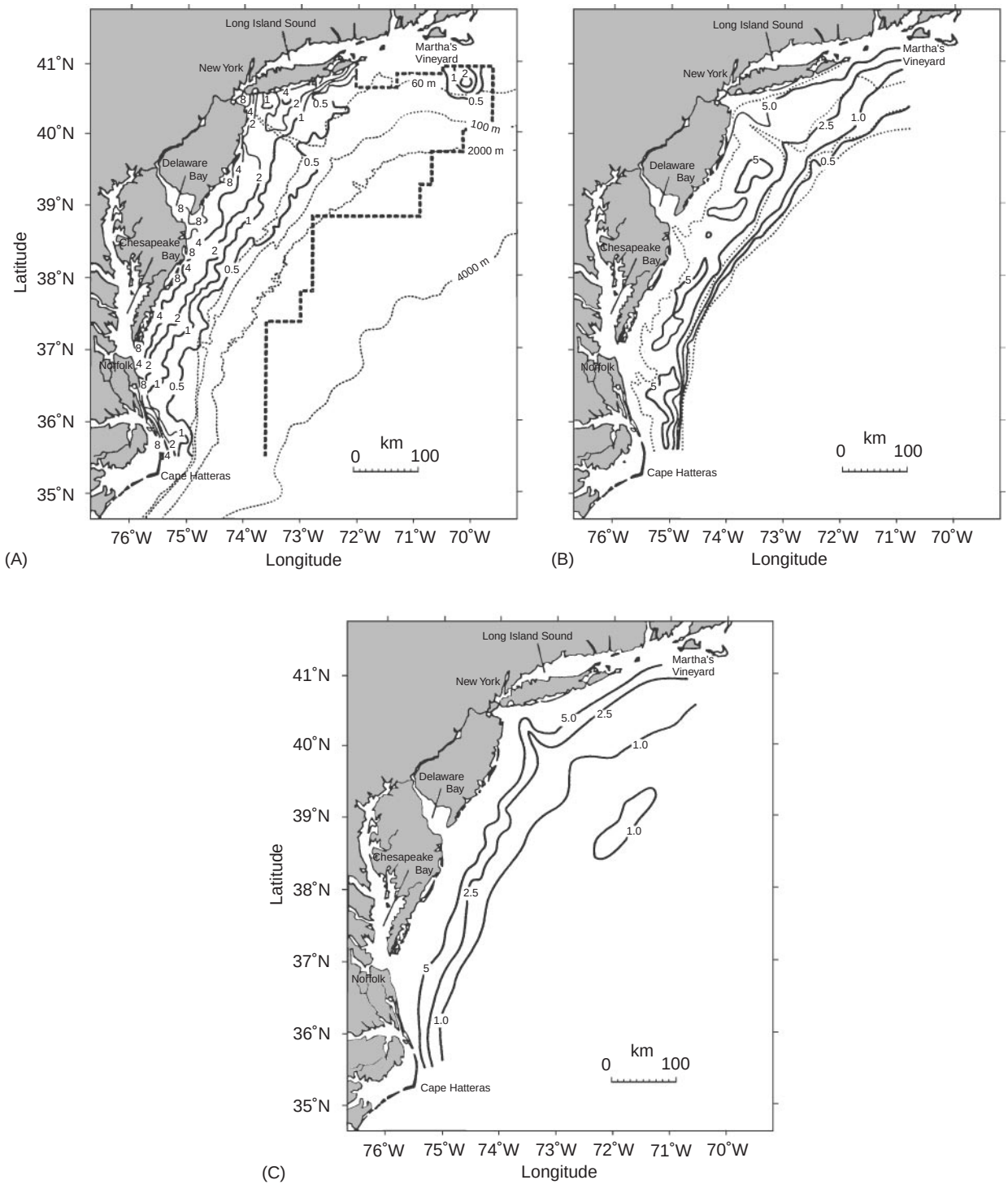

Figure 3 The observed (A) and simulated biomass (μg chl l^{-1}) at the surface of the Mid-Atlantic Bight during 10 April 1979, as seen by the Coastal Zone Color Scanner (CZCS) and modeled by simple food webs of (B) one and (C) two functional groups of phytoplankton within the same barotropic circulation model, under wind forcing measured at John F. Kennedy Airport.

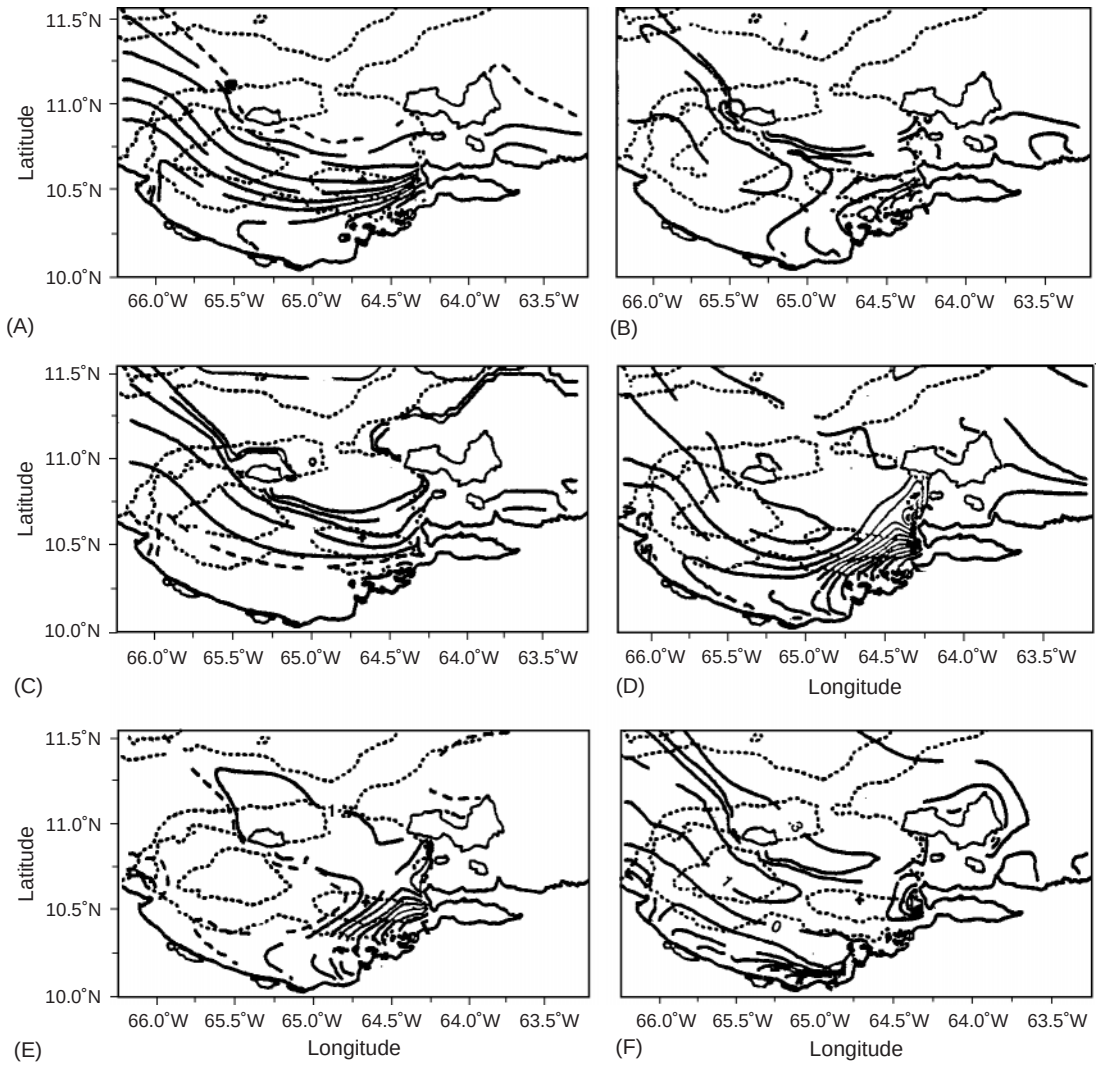

Figure 4 The simulated spring distributions within a two-layered baroclinic circulation model, under wind forcing measured during February–April 1996–1997 at Margarita Island, of (A) near-surface chlorophyll ($\mu g\ l^{-1}$), (B) water column net primary production (mg C $m^{-2}\ d^{-1}$), (C) 1% light depth (m), and, at ~ 25 m depth of (D) total CO_2 (μmol DIC kg^{-1}), (E) nitrate (μmol $NO_3\ kg^{-1}$), and (F) ammonium (μmol $NH_4\ kg^{-1}$) around the CARIACO time-series site (+) on the Venezuelan shelf.

total spring production was exported to the deep sea, compared to prior estimates of $\sim 50\%$.

Southern Caribbean Sea

The second biophysical model of the Venezuelan shelf was again wind-forced with a mesh of ~ 4 km within 200 km of the land boundary, but the seaward boundary now extended ~ 1400 km out from the coast, intersecting Puerto Rico and Cuba, with a telescoping mesh of maximal size of ~ 110 km. A western boundary current was assumed to flow east–west along the model's shelf-break at a depth of ~ 100 m (**Figure 4**). Both barotropic and baroclinic flow fields were computed from a two-layered, linearized circulation model – i.e., again without advection of momentum and ignoring tidal forces. The ecological formulation over 30 depth intervals is also more complex, with the additional state variables of carbon dioxide, labile and refractory dissolved organic matter, bacteria, and zooplankton fecal pellets, as well as nitrate, ammonium, and light-regulated diatoms.

During spring upwelling of $8\ m\ d^{-1}$ near the coast and $3\ m\ d^{-1}$ offshore at a time-series site (' + ' on **Figure 4**), the thermal fields of the physical model match satellite and ship estimates of surface temperature in February–April 1996–1997. Within the three-dimensional flow field, the steady solutions of detrital effluxes from a simple food web of diatoms, adult calanoid copepods, and the ammonifying/nitrifying bacteria are also $\sim 91\%$ of the mean spring observations of settling fluxes of particulate carbon

caught by a sediment trap at a depth of ~ 240 m, moored in the Cariaco Basin (+). At this station, the other state variables of the coupled models are within $\sim 71\%$ of the chlorophyll biomass (**Figure 4A**), $\sim 89\%$ of the average ^{14}C net primary production of $2.0\,g\,C\,m^{-2}\,d^{-1}$ (**Figure 4B**), $\sim 80\%$ of the light penetration (**Figure 4C**), and 97% of the total CO_2 stocks (**Figure 4D**). No data were then available for nitrate, ammonium, or satellite color.

When the Intertropical Convergence Zone of the North Atlantic winds moves north in summer, local winds along the Venezuelan coast slacken. Within one summer case of the model with weaker wind forcing, the simulated net primary production is only 14% of that measured in August–September, while the predicted detrital flux is then 30% of the observed. Addition of a diazotroph state variable (**Figure 1**), with another source of 'new' nitrogen via nitrogen fixation rather than upwelled nitrate, would remedy the seasonal deficiencies of the biological model, attributed to use of a single phytoplankton groups. We explore such a scenario in the last case.

West Florida Shelf

All of the terms eqns [3]–[5] and [9] were maintained in a recent series of wind-forced barotropic circulation models of the West Florida shelf, with horizontal grid meshes of ~ 4–9 km and 16–21 vertical levels over the water column. Open boundary conditions of flow at a depth, H, of ~ 1500 m in the Gulf of Mexico basin, as well as on the shelf, were of the radiation form [18], where C is the speed of gravity waves (i.e., $(gH)^{1/2}$) and u is determined from the adjacent interior grid points of the model.

$$\frac{\partial u}{\partial t} = C\frac{\partial u}{\partial x} \qquad [18]$$

When the additional constraint is imposed that the depth-integrated transport across these boundaries is zero, as in the shelf-break condition of the Mid-Atlantic Bight (**Figure 2**), fluxes of water within the surface and bottom Ekman layers cancel each other. Since biochemical variables exhibit nonuniform vertical profiles, however, the net influx of nutrient within the bottom layer of the embedded ecological model may instead be balanced by a net efflux of plankton within the surface layer. Prior one-dimensional models of element cycling by eight functional groups of phytoplankton on the West Florida shelf concerned most of the state variables of **Figure 1**, while the three-dimensional results, shown here, consider just the transport of a harmful algal bloom (**Figure 5**), with diel migration of the dinoflagellate *Gymnodinium breve*.

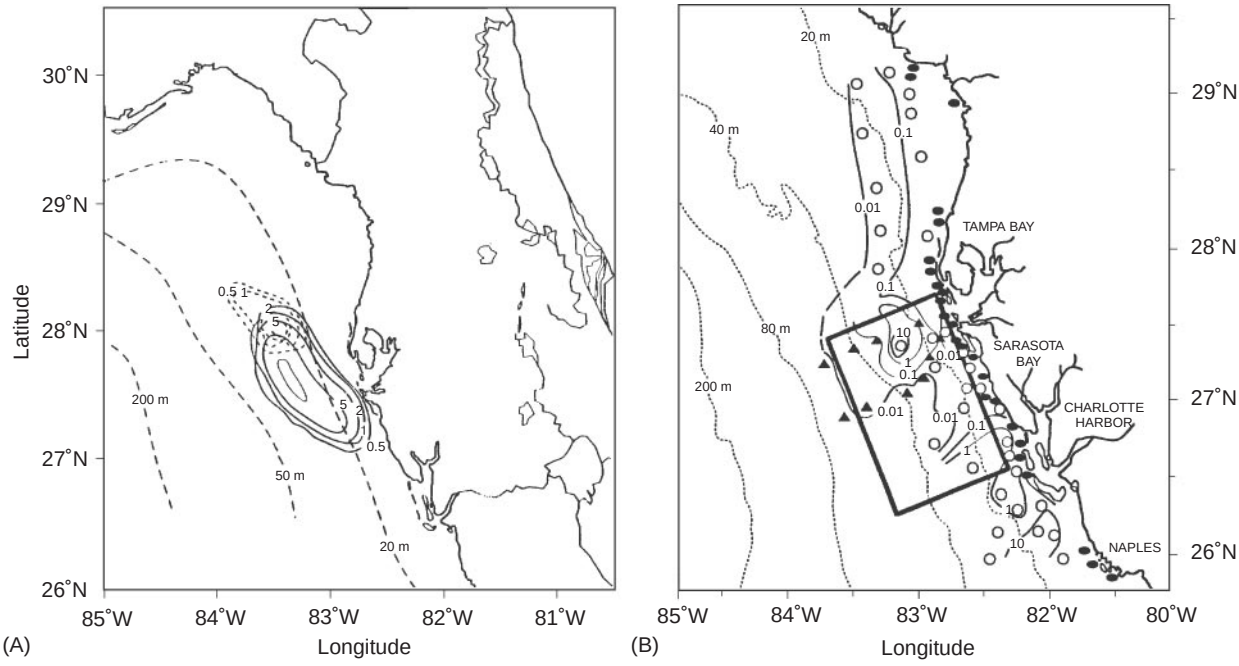

Figure 5 The (A) simulated and (B) observed daily trajectories on the West Florida shelf of a near-surface red tide (10^5 cells $l^{-1} = 1\mu g$ chl l^{-1}) of *Gymnodinium breve*. The model's population is growing at a maximal rate of $\sim 0.15\,d^{-1}$ with vertical migration and nocturnal convective mixing, during sunrise (06:00) on 20 December 1979, after initiation on 25 November (dashed contours), and under forcing of a barotropic circulation model by winds measured at the Tampa International Airport. The offshore observations were made during 10–11 December 1979 (solid triangles) and 19–21 December 1979 (open circles) in relation to landfalls of red tides sampled (solid circles) on piers and bridges during 11/25/79–2/8/80.

Once a red tide of *G. breve* is formed, after DON supplied from nitrogen-fixers of our one-dimensional model, its simulated trajectory over 16 vertical levels during December 1979 (**Figure 5A**) matches repeated shipboard and helicopter observations (**Figure 5B**) of this dinoflagellate bloom at the surface of the West Florida shelf, if one samples the model at sunrise after nocturnal convective mixing: at noon, the simulated red tide instead aggregates in a subsurface maximum, as observed during additional time-series studies.

Under the predominantly upwelling-favorable winds of fall/winter, the circulation model yields a positive w of ~ 0.5–$1.0\,\mathrm{m\,d^{-1}}$ within the red tide patch and of 1.0–$2.0\,\mathrm{m\,d^{-1}}$ at the coast. In another model case, without the vertical downward migration of *G. breve* at a speed of $\sim 1\,\mathrm{m\,h^{-1}}$ to avoid bright light, the model's surface populations then did not replicate the data; they were instead advected farther offshore than the *in situ* populations. It appears that in the 'real world' *G. breve* spent most of their time in the lower layers of the water column, before ascending to be sampled by ship and helicopters during daylight at the sea surface.

Furthermore, within the bottom Ekman layer, the simulated red tide is advected onshore, mimicking observations of shellfish bed closures on the barrier islands. Thus, the coupled models suggest that, upon maturation of a red tide from successful competition among functional groups of the phytoplankton community (**Figure 1**), vertical migration of *G. breve* in relation to seasonal changes of summer downwelling and fall/winter upwelling flow fields then determines the duration and intensity of red tide landfalls along the beaches of the west coast of Florida.

Prospectus

Other regional models of varying ecological and physical realism have been constructed for numerous shelf regions. They are mainly classic *N–P–Z* formulations, however, such that they may be improved with inclusion of a larger number of ecological state variables. Simply adding biochemical and physical variables for the next generation of coupled regional models is not sufficient, because the initial and boundary conditions will always be poorly known. Like models of the weather on land, such predictive models must be continually validated with data to correct for the poor knowledge of these conditions.

Given the expense of shipboard monitoring programs, a few bio-optical moorings (e.g., fluorometers or remote sensors (**Figure 1**)), are the most likely sources of such updates for the ecological models. Furthermore, the veracity of the underlying circulation models must be maintained with a complete suite of buoyancy flux measurements at the same moorings, to derive the baroclinic contributions important to the regional flow fields. For example, the barotropic calculations of the West Florida shelf case did not match current meter observations during summer on the outer shelf. The bio-optical implications of regional physical/ecological models driven by time-dependent density fields must be included in future simulation analyses.

See also

Elemental Distribution: Overview. El Niño Southern Oscillation (ENSO) Models. Forward Problem in Numerical Models. Inverse Models. Lagrangian Biological Models. Population Dynamics Models.

Further Reading

Csanady GT (1982) *Circulation in the Coastal Ocean*. Dordrecht: Riedel.

Heaps NS (1987) *Three-Dimensional Coastal Ocean Models*. Coastal and Estuarine Series 4. Washington, DC: American Geophysical Union.

Mooers CN (1998) *Coastal Ocean Prediction*. Coastal and Estuarine Series 56. Washington, DC: American Geophysical Union.

Riley GA, Stommel H and Bumpus DF (1949) Quantitative ecology of the plankton of the western North Atlantic. *Bulletin of Bingham Oceanographic College* 12: 1–169.

Steele JH (1974). *The Structure of Marine Ecosystems*. Cambridge, MA: Harvard University Press.

Walsh JJ (1988). *On the Nature of Continental Shelves*. San Diego, CA: Academic Press.

REMOTELY OPERATED VEHICLES (ROVs)

K. Shepherd, Institute of Ocean Sciences, British Colombia, Canada

doi:10.1006/rwos.2001.0302

Introduction

Remotely operated vehicles (ROVs) are vehicles that are operated underwater and remotely controlled from the surface. All types of this vehicle are